Journal of Materials Chemistry A

Accepted Manuscript

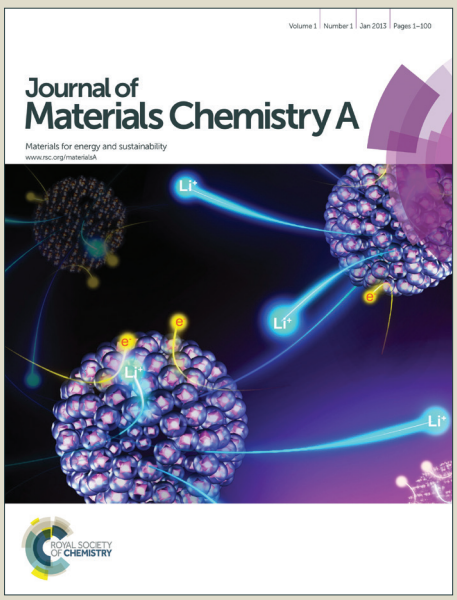

ROYAL SOCIETY OF CHEMISTRY

www.rsc.org/materialsA

Journal of

Materials Chemistry A

RSCPublishing

ARTICLE

Enhancing CO_2 separation performance of composite membrane by incorporation of amino acid-functionalized graphene oxide

Qingping Xin[a,b], Zhao Li[a], Congdi Li[a], Shaofei Wang[a,b], Zhongyi Jiang[a,b], Hong Wu[*,a,b,c], Yuan Zhang[d], Jing Yang[e] and Xingzhong Cao[e]

Cite this: DOI: 10.1039/x0xx00000x

Received 00th January 2012,
Accepted 00th January 2012

DOI: 10.1039/x0xx00000x

www.rsc.org/

The composite membranes are fabricated by incorporating amino acid-functionalized graphene oxide (GO-DA-Cys) nanosheets into sulfonated poly (ether ether ketone) (SPEEK) polymer matrix. Graphene oxide (GO) nanosheets are functionalized with amino acids through a facile two-step method by using dopamine (DA) and cysteine (Cys) in succession. CO_2 separation performance of the as-prepared membranes is evaluated for CO_2/CH_4 and CO_2/N_2 systems. GO nanosheets increase more tortuous paths for the larger molecules, enhancing diffusivity selectivity. Amino acid with the carboxylic acid groups and primary amine groups simultaneously enhances solubility selectivity and reactivity selectivity. Accordingly, CO_2 molecules can transport quickly with the enhanced selectivity. When the GO-DA-Cys content is 8 wt %, the optimum separation performance is achieved at the GO-DA-Cys content of 8 wt % with selectivities of 82 and 115 for CO_2/CH_4 and CO_2/N_2, respectively, and CO_2 permeability of 1247 Barrer, significantly surpassing the Robeson upper bound reported in 2008. Besides, the mechanical and thermal stabilities of the composite membranes are also improved compared with pristine SPEEK membrane.

1. Introduction

Composite membranes emerge as an effective solution to overcome the Robeson's upper bound trade-off limit existing in polymeric membrane for gas separation.[1-16] It is believed that this emerging approach is viable to synergistically combine the advantageous features of both phases and overcome trade-off limit. In composite membranes, inorganic fillers were embedded in polymer matrix. Until now, carbon molecular sieves,[6] zeolites,[17,18] mesoporous materials,[19] activated carbons,[20] carbon nanotubes[21] and metal-organic frameworks[22] have been extensively used for composite membranes fabrication. Particulate inorganic materials are most commonly used as dopants in composite membranes. Recently, interest has risen in sheet-shaped fillers which are called flakes or lamellar materials.[23-25]

Sheet-shaped materials have been applied as inorganic fillers in composite membranes.[23-30] Sheet-shaped fillers usually have a high aspect ratio with a thickness at nanoscale which allows casting of thin composite membranes with horizontally oriented sheets. Galve *et al* introduced the sheet-shaped microporous titanosilicate into copolyimide membranes.[28] The sheet-shaped particles were horizontally orientated in the membrane and the H_2/CH_4 selectivity was found to be increased by 76 %. The addition of nanosheets can disrupt the packing of polymer chains and tune the size of free volume elements, thus increasing gas diffusivity and diffusivity selectivity.[31,32] Graphene oxide (GO) as a typical sheet-shaped materials has attracted much attention for its multiple advantageous features such as high aspect ratio (>1000), facile synthesis, easily tunable surface functionalization, high mechanical and thermal properties. In GO-doped membranes the small molecule gases can go through the defects of GO nanosheets or through the interspace between the layers of the stacked GO nanosheets. Furthermore, the high aspect ratio of GO nanosheets increase longer and more tortuous paths for the larger molecule that cannot easily pass through the pores, and thereby effectively decrease the permeability of the larger molecule.[33,34] It is expected that membranes containing thin nanosheets will lead to high separation performances. Jin *et al* prepared graphene oxide-doped composite membranes for efficient CO_2 separation and obtained a high CO_2/N_2 selectivity of 91 due to the enhanced selective diffusion of gases through the membranes.[31]

Amino acid was applied for efficient gas separation recently.[35-39] Matsuyama *et al* found that [35-37] the strong water holding ability of

amino acid resulted in the large absorption amount of CO_2 and a large concentration gradient. The large concentration gradient provided a large driving force for CO_2-complex transport through the membrane and increased CO_2 permeability. Polar carboxylic acid group (-COOH) on amino acid possesses excellent affinity to quadrupole moment gases like CO_2, and it has been confirmed to be effective to achieve high CO_2 permeability and CO_2/gas selectivity due to the increase of solubility selectivity.[40-44] In addition, basic group (primary amine) on amino acids is good candidates to improve both CO_2 permeability and CO_2/gas selectivity through the reversible reactions between acidic gas CO_2 and amine groups in the membranes.[45-53]

Sulfonated poly(ether ether ketone) (SPEEK) is a potential membrane material for gas separation.[53,54] In this study, zwitterionic amino acid-grafted graphene oxide nanosheets are incorporated into SPEEK to fabricate composite membranes for gas separation. Nanosheets fillers lead to more tortuous pathways for the larger molecules, accordingly enhancing diffusivity selectivity. Moreover, grafting amino acid with amine groups and carboxyl groups onto the GO fillers is expected to remarkably increase the content of CO_2 interaction sites in the membranes, leading to an increment in both gas reactivity and solubility selectivity. The membrane morphology, polymer chain rigidity, membrane free volume property, mechanical property and thermal stability are characterized and the separation performance is explored for CO_2/CH_4 and CO_2/N_2 systems.

2. Experimental

2.1 Chemicals and materials

Poly(ether ether ketone) (PEEK) was gained from Victrex High-performance Materials (Shanghai, China) Co., Natural flake graphite (2500 mesh) was purchased from Qingdao Tianhe Graphite Co. Ltd. (Shandong, China).Ltd. 3-2-(3,4-dihydroxyphenyl)ethylamine (Dopamine) was purchased from Yuancheng Technology Development Co., Ltd. (Wuhan, China). Tris(hydroxymethyl) aminomethane (Tris) was purchased from Sigma-Aldrich. Potassium permanganate ($KMnO_4$) and hydrochloric acid were purchased from Tianjin Jiangtian Ltd. (Tianjin, China). Cysteine, hydrogen peroxide aqueous solution (H_2O_2, 30 wt%), calcium chloride dihydrate ($CaCl_2{\cdot}2H_2O$), sodium nitrate ($NaNO_3$), sulfuric acid (H_2SO_4, 98 wt.%), absolute ethanol and N,N-Dimethyl acetamide (DMAc) were of analytical grade and purchased from Tianjin Guangfu Fine Chemical Research Institute (Tianjin, China).

Sulfonated poly(ether ether ketone) (SPEEK) (Fig. 1) with sulfonation degree 63 % was prepared by direct sulfonation of PEEK.[51] PEEK was firstly dried in oven at 80 °C for 24 h before sulfonation. Then, the dried PEEK (14 g) was gradually dissolved into 100 mL sulfuric acid (H_2SO_4, 98 wt %) in a three-neck flask for about 4.5 h at room temperature, followed by vigorous stirring at 10 h. Afterward, the polymer solution was gradually precipitated into water under mechanical agitation. Finally, the polymer precipitate was washed several times with deionized water until pH reached neutral and then dried first at room temperature for one week and then at 60 °C for another 24 h. The degrees of sulfonation (DS) were determined through acid-base titration method.

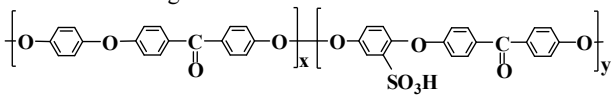

Fig. 1. Chemical structure of SPEEK.

2.2 Preparation of amino acid-functionalized graphene oxide nanosheets

Pristine graphene oxide (GO) was prepared by Hummers method as reported.[55] Amino acid-functionalized graphene oxide nanosheets (GO-DA-Cys) are obtained using dopamine (DA) and cysteine (Cys) in succession under mild conditions.[53,56] The process can be divided into two steps (see Fig. 2, and the detailed description is shown in Supporting materials), and the intermediate product dopamine modified graphene oxide was designated as GO-DA.

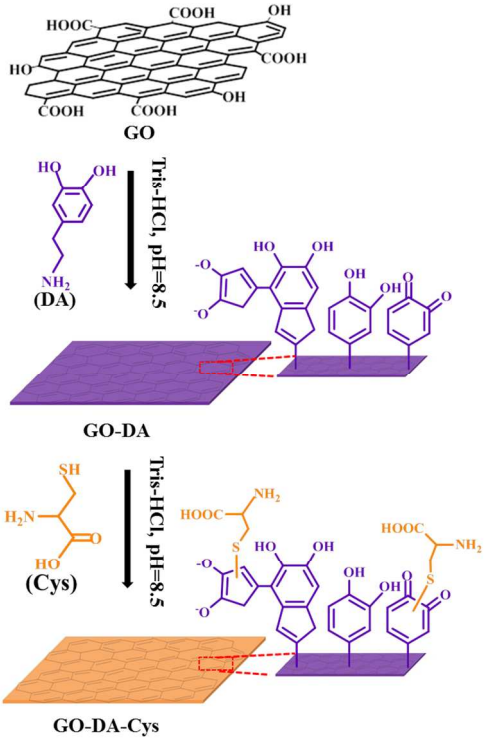

Fig. 2. The grafting mechanism of dopamine and cysteine on GO nanosheets.

2.3 Fabrication of membranes

SPEEK (0.6 g) was dissolved in DMF (8 g) at room temperature. A measured amount of nanosheets was dispersed in DMF (4 g) and the resulting suspension was added into SPEEK-DMF solution under vigorously stirring for 24 h to get a fine dispersion of nanosheets in the polymer solution. After degasification, the mixture was poured on a clean glass plate and heated overnight at 60 °C for 12 h, followed by annealing at 80 °C for another 12 h. The membranes were peeled off from the glass plate, dried under vacuum at 60 °C for 24 h and designated as SPEEK/GO-X, SPEEK/GO-DA-X and SPEEK/GO-DA-Cys-X, respectively, and X (=2, 4, 6 or 8) was the weight percentage of the nanosheets content relatively to the weight of SPEEK. The amounts of DA and cysteine on the GO were determined by TGA. Unfilled SPEEK membrane was also fabricated for comparison. The thickness of the as-prepared flat sheet homogeneous membranes was in the range of 45~70 μm.

2.4 Characterization

2.4.1 Characterization of membranes

Positron annihilation lifetime spectroscopy (PALS) was used to investigate the free volume property of the membranes as reported.[51] On assumption that the location of o-Ps occurs in a sphere potential well surrounded by an electron layer of a constant thickness Δr (0.1656 nm), radius of free volume cavity (r_3) was calculated from the pick-off annihilation lifetime of o-Ps (τ_3) by the following semi-empirical Eq. (1).

$$\tau_3 = \frac{1}{2}\left[1 - \frac{r_3}{r_3 + \Delta r} + \left(\frac{1}{2\pi}\right)\sin\left(\frac{2\pi r_3}{r_3 + \Delta r}\right)\right]^{-1} \quad (1)$$

The apparent fractional free volume (FFV) of the equivalent sphere could be calculated by using Eq. (2).

$$FFV = \frac{4}{3}\pi r_3^3 I_3 \quad (2)$$

Water state in membranes was determined following the reported procedure.[10] The "humidified" weight (m_1, mg) of each membrane was weighed after gas permeation, and then each membrane was heated at 100 °C in a vacuum oven to fully remove free water. Each membrane was reweighed (m_2, mg) at this step. After the membrane was dried at 150 °C, they were weighed again to determine their "dried" weight (m_0, mg). In this way, the content of total water (W_t, %), free water (W_f, %) and bound water (W_b, %) were obtained by $W_t = (m_1-m_0)/m_0\times100$ %, $W_f = (m_1-m_2)/m_0\times100$ %, $W_b = (m_2-m_0)/m_0\times100$ %, respectively.

2.5 Gas permeation tests of flat sheet homogeneous membranes

Pure gas (CO_2, CH_4 and N_2) and mixed gas (CO_2/CH_4 = 30/70 vol% and CO_2/N_2 = 10/90 vol%) permeation experiments were conducted at 25 °C based on the conventional constant pressure/variable volume gas permeation system under dry or wet conditions. The detailed description on experimental apparatus and procedures can be found in our previous publications.[10,53] Prior to contacting the membranes, both the feed gas and sweep gas were saturated with water vapor by passing through a water-containing bottle at 35 °C and then passing through an empty bottle at room temperature (about 25 °C) to remove the condensate water.The permeability (P_i, Barrer, and 1 Barrer = 10^{-10} cm^3 (STP) cm/(cm s cmHg)) of either gas was obtained from the average value of at least twice measurements, by using the equation (3):

$$P_i = \frac{Q_i l}{\Delta p_i A} \quad (3)$$

where Q_i is the volumetric flow rate of gas 'i' (cm^3/s) at standard temperature and pressure (STP), Δp_i is the transmembrane pressure difference (cmHg), and A is the effective membrane area, 12.56 cm^2. The pure gas ideal selectivity (α_{ij}) was calculated by equation (4):

$$\alpha_{ij} = \frac{P_i}{P_j} \quad (4)$$

The mixed gas separation factor ($\alpha_{i/j}^*$) was calculated by the following equation (5):

$$\alpha_{ij}^* = \frac{(y_i/y_j)}{(x_i/x_j)} \quad (5)$$

where y and x are the compositions of i and j on the permeate and feed sides, respectively.

To further elucidate the gas transport mechanism in membranes, diffusivity and solubility coefficients of membranes were measured by the time-lag method.[52] Before test, all the membranes were evacuated at least 8 h to fully remove dissolved species. For each membrane the gases were measured in the order of N_2, CH_4 and CO_2.

3. Results and discussion

3.1 Characterization of the nanosheets

The typical sheet-shaped morphology of GO, GO-DA and GO-DA-Cys is characterized by TEM (Fig. 3(a-c)). The low optical contrast indicates that GO is fully exfoliated into individual and ultrathin nanosheets. The morphologies of GO-DA and GO-DA-Cys are modestly changed in comparison with pristine GO. The sizes of GO-DA and GO-DA-Cys nanosheets become smaller than that of GO. It can be inferred that the ultrasound process leads to the breaking of GO nanosheets into smaller fragments.

FTIR, XPS and TGA are used to investigate the surface composition of the amino acid-functionalized graphene oxide. As shown by the FT-IR spectra (Fig. 3(d)), characteristic peaks in GO spectra are observed at 3453, 1739, 1577, 1396, 1209 and 1083 cm^{-1}, which are associated with the stretching vibration of C-OH, stretching vibration of C=O, asymmetrical stretching vibration of COO, in-plane bending vibration of C-OH, stretching vibration of C-O (epoxy) and stretching C-O (alkoxy), respectively. Accordingly, the existence of oxygen-containing groups on GO nanosheets is confirmed, including carboxyl, hydroxyl and epoxy. GO-DA displays FTIR spectrum including the distinct peaks of polydopamine at about 1477 cm^{-1}, 1600 cm^{-1} and 1270 cm^{-1}, which correspond to the N-H deformation vibration, C=C and C-N stretching vibration, respectively. These characteristic bands suggest that the dopamine is successfully introduced onto the GO nanosheets surface. Amino acid-functionalized graphene oxide displays the distinct peak at about 675 cm^{-1} which is associated with the C-S stretching vibration in cysteine. In comparison, the peak corresponding to C-S is notably in GO-DA-Cys, indicating that cysteine is successfully introduced onto GO-DA nanosheets. XPS is utilized to investigate surface composition of the nanosheets (Fig. 3(e)). The XPS data of GO, GO-DA and GO-DA-Cys nanosheets is listed in Table S1 (see supporting materials). The content of newly appeared nitrogen (N1s) from PDA is about 6.5%. After the GO is amino acid-functionalized, the content of nitrogen (N1s) increases to 13.6%, while the content of sulfur (S2p) is 11.0% attributed to cysteine. For the characteristic signal of PDA, N1s at 400 eV is obviously observed in comparison with pristine GO, indicating the successful grafting of PDA layer from the surfaces. In addition, the presence of sulfur specie at 168 eV further confirms that cysteine is indeed functionalized onto the GO surface. The thermal stability of nanosheets (GO-DA and GO-DA-Cys) is analyzed by thermogravimetry analysis (TGA, Fig. 3(f)). The samples exhibit two weight loss stages, and the first weight loss stage between 50 °C and 195 °C is attributed to absorbed water. The second weight loss stage (from 230 °C to 700 °C) is ascribed to the decomposition of the coating layer, and the content of grafted cysteine is about 12.6 %.

The XRD patterns of the GO, GO-DA and GO-DA-Cys nanosheets are recorded to further investigate their nanostructure (Fig. 3(g)). The pristine GO nanosheets have a strong peak at 2θ = 10.10°, corresponding to the (001) reflection and the d-spacing of 0.87 nm. Compared with pristine GO nanosheets, the d-spacings of GO-DA and GO-DA-Cys nanosheets increase to 1.08 nm and 1.43 nm at a peak of 8.14° and 6.17°, respectively. This increase corroborates the introduction of dopamine and cysteine molecules onto GO nanosheets, which enlarge the d-spacing.

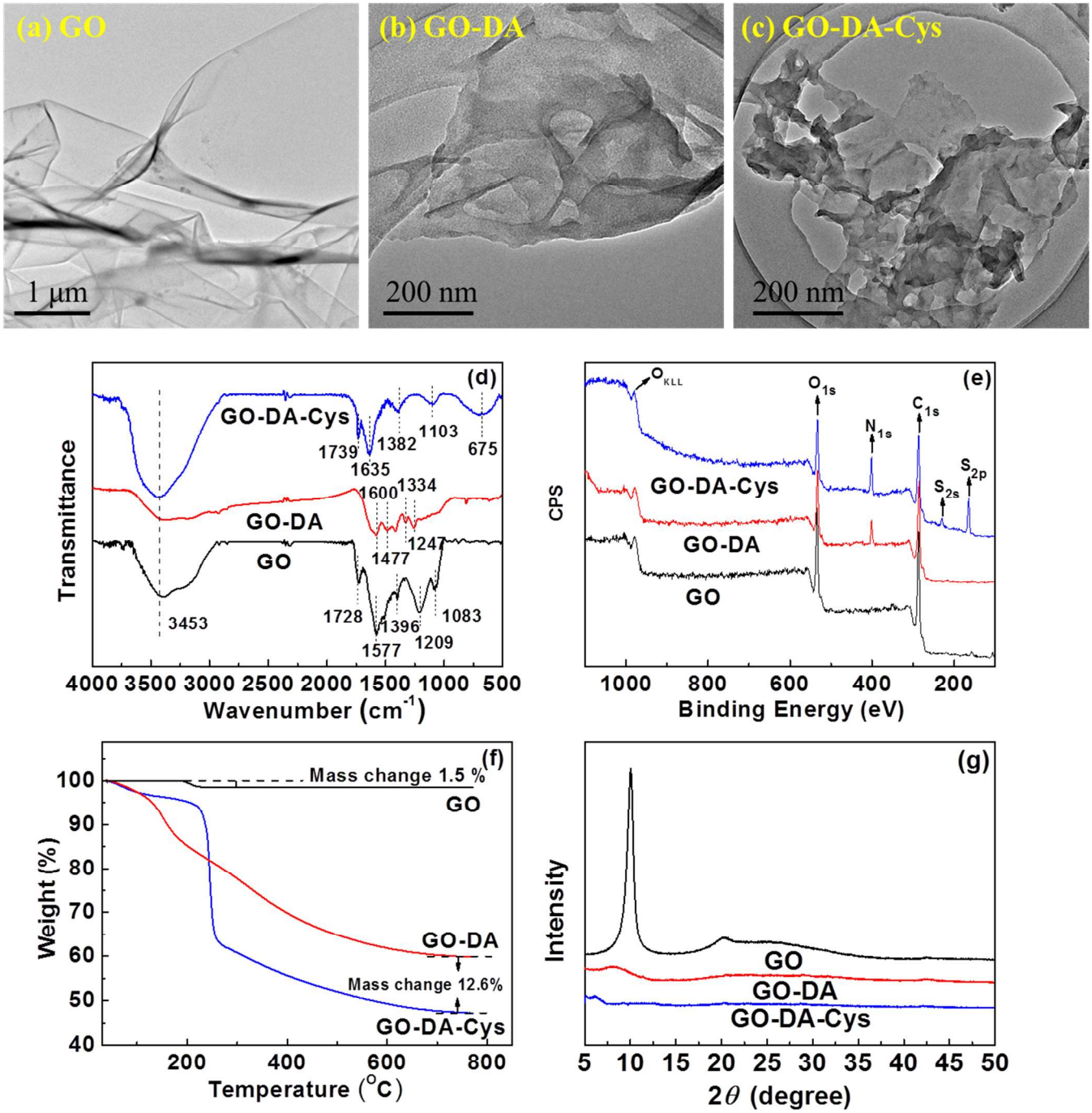

Fig. 3. Characterization of GO, GO-DA, and GO-DA-Cys: (a) TEM image of GO, (b) TEM image of GO-DA, (c) TEM image of GO-DA-Cys nanosheets, (d) FTIR spectra, (e) XPS curves, (f) TGA curves, and (g) XRD curves.

3.2 Characterization of the membranes

The cross-section SEM images of the membranes are exhibited in Fig. 4. Composite membranes doped with unmodified GO show that GO nanosheets are poorly distributed in the SPEEK matrix and has poor compatibility with polymer matrix at loading of 8 wt % (Fig. 4 (d, e, f)). However, it can be seen from Fig. 4(g, h, i) and (j, k, l) that the nanosheet-polymer interfacial adhesion is improved by introducing dopamine and cysteine on GO. Furthermore, Fig. 4(g, h, i) and (j, k, l) display that modified nanosheets are completely surrounded by SPEEK matrix and no obvious voids form, suggesting that dopamine and cysteine on the surface of GO improve interface compatibility between modified nanosheets and SPEEK matrix. The improved interface compatibility is mainly due to the acid-base interactions existing between the amine groups on nanosheets and sulfonic acid groups from SPEEK matrix.

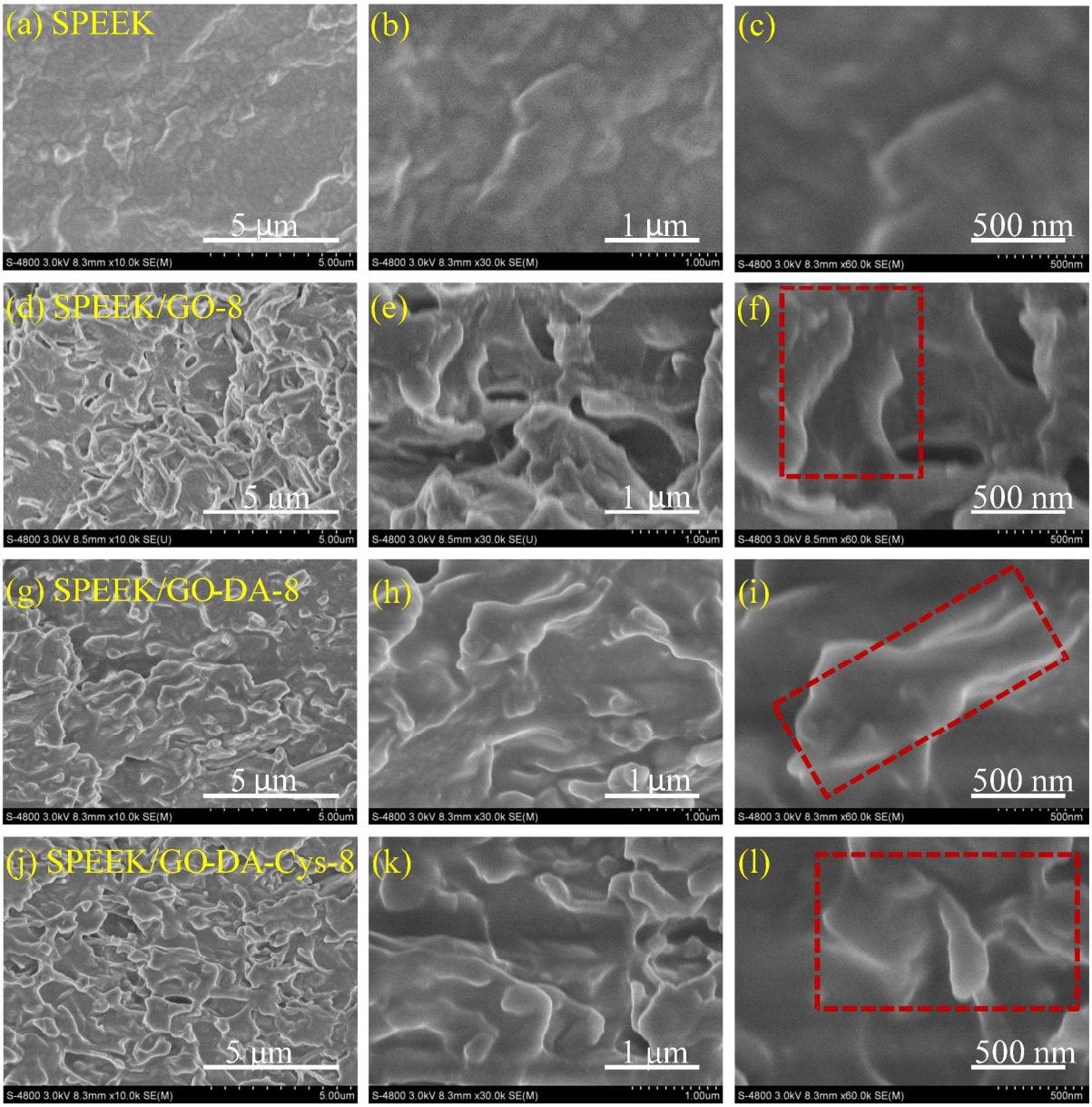

Fig. 4. FESEM images of the cross-section of the unfilled membrane and the composite membranes: (a, b, c) unfilled SPEEK membrane, (d, e, f) SPEEK/GO-8, (g, h, i) SPEEK/GO-DA-8, and (j, k, l) SPEEK/GO-DA-Cys-8.

FTIR spectra of composite membranes are shown in Fig. 5(a). The major vibration peaks associated with the O=S=O groups from SPEEK at 1022, 1078 and 1225 cm^{-1} are found in all the composite membranes. The composite membranes exhibit a stronger peak at 1645 cm^{-1} than unfilled SPEEK membrane which is attributed to the vibration of heteroaromatic ring in nanosheets. Compared with FTIR spectrum of the unfilled SPEEK membrane, FTIR spectra of membranes loaded with GO and GO-DA-Cys clearly show the representative peaks of carboxylic acid groups at 3460 cm^{-1} and 1739 cm^{-1}corresponding to -OH and C=O stretching vibrations, respectively. Moreover, a peak at 1735 cm^{-1} (related to the stretching vibration of C=O) in SPEEK/GO-DA-Cys membrane is shifted to the lower wave number (1720 cm^{-1}), indicating that electrostatic interaction and hydrogen bonding are formed between sulfonic acid group and amine groups/carboxyl groups after the incorporation of cysteine functionalized nanosheets.

The crystalline properties of membranes are provided by WXRD in Fig. 5(b), which shows a crystalline reflection of the SPEEK backbone in all the membranes at 2θ= 8–21°.[57] Compared with the unfilled SPEEK membrane, the composite membranes show a declined intensity of this peak. Such phenomena are ascribed to the presence of nanosheets, which hinder the crystallization of the backbone. As the content of graphene oxide increases, the crystallinity of SPEEK/GO-DA-Cys membranes decreases. The peak is more weakened in the membrane loaded with 8 wt % cysteine-grafted GO because the functionalized GO has a more homogeneous dispersion in polymer matrix through mutual interactions and space interference in comparison with SPEEK/GO-8 membrane and SPEEK/GO-DA-8 membrane. In addition, the diffraction peaks of the nanosheets disappear in the WXRD curves due to the overlap of the crystallization peak of SPEEK.[58]

TGA is used to analyse the thermal stability of the membranes. The weight loss rate of the composite membranes is slower than that of unfilled SPEEK membrane as shown in Fig. 5(c). The decomposition rates of SPEEK/GO-DA-8 and SPEEK/GO-DA-Cys-8 are slightly faster than that of SPEEK/GO-8 due to more functional

groups coated onto GO nanosheets. The incorporation of nanosheets enhances the thermal stability of composite membranes.

Good mechanical property is crucial for membranes application. Both the tensile strength and Young's modulus of composite membranes are significantly enhanced compared with those of unfilled SPEEK membrane (Table S2, see supporting materials). The enhancement is ascribed to the increased chain rigidity imparted by the addition of nanosheets and interfacial interaction.[54] Moreover, compared with SPEEK/GO-8 and SPEEK/GO-DA-8 membranes, the SPEEK/GO-DA-Cys-8 membrane shows increased Young's modulus and tensile strength, respectively, mainly due to the increased interfacial interaction between GO-DA-Cys and SPEEK.

The static contact angles of membranes are shown in Fig. 5(d). The unfilled SPEEK membrane exhibits a water contact angles of 74.5º. The water contact angles decrease with the nanosheets loading increasing, indicating an increased hydrophilicity of all the composite membranes. The contact angles of SPEEK/GO-DA-Cys composite membranes are the lowest in all composite membranes at the same loading, indicating the highest hydrophilic composite membranes. The SPEEK/GO-DA-Cys-8 membrane with a water contact angles of 55.9 ° exhibits the highest hydrophilicity. The abundant hydrophilic groups such as carboxyl groups or amine groups from GO-DA-Cys nanosheets could improve SPEEK membrane surface hydrophilic.

The glass transition temperature (T_g) of membranes is shown in Table 1. The unfilled SPEEK membrane displays a T_g of 161.8 °C. All the composite membranes show an increased T_g in comparison with unfilled SPEEK membrane (Table S3). Compared with composite membranes doped with GO-DA nanosheets, SPEEK/GO-DA-Cys composite membranes show an increased T_g, indicating a more rigidity of polymer chains due to the acid-base interactions.

The free volume parameters of the membranes are listed in Table 1. The size of the free volume cavity (r_3) is slightly changed for both unfilled membrane and composite membranes, while compared with unfilled SPEEK membrane, the composite membranes loaded with GO-DA-Cys show an increased fractional free volume (FFV). The FFV increases with the GO-DA-Cys content increasing. This increased FFV can lead to an increase of gas permeability.

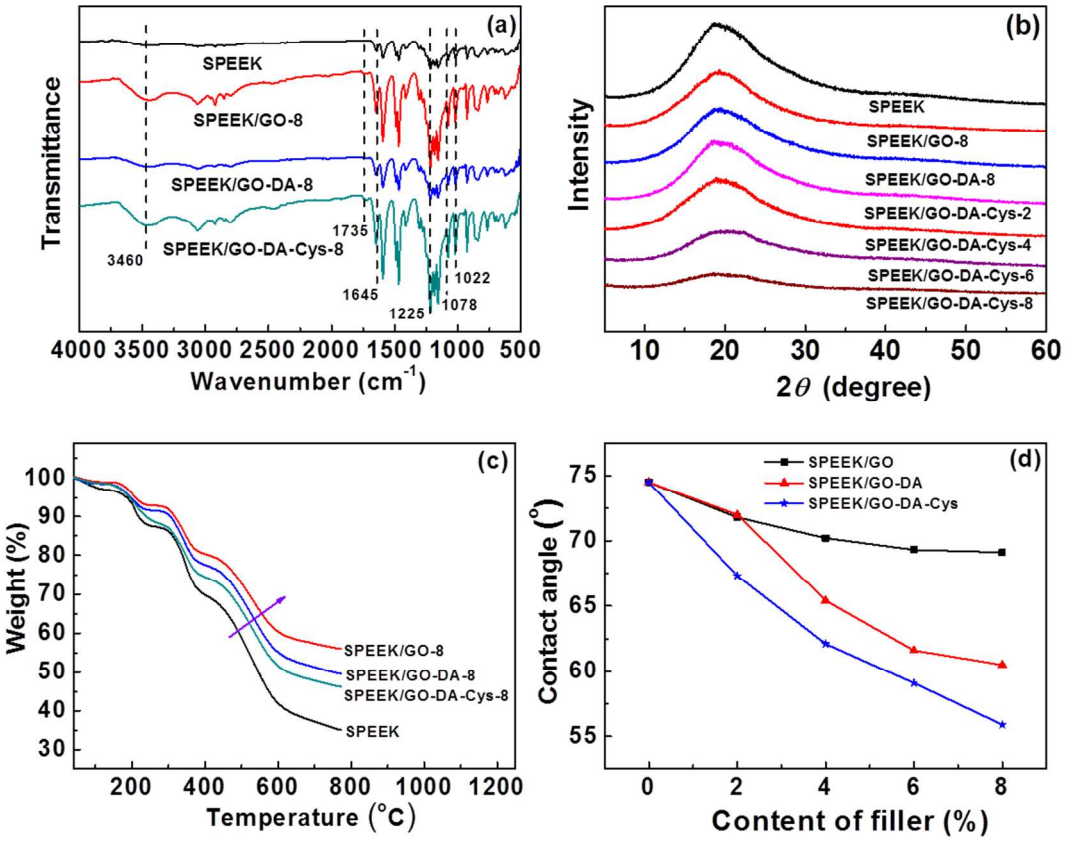

Fig. 5. (a) FTIR spectra, (b) WXRD, (c) TGA, and (d) water contact angles curves of membranes.

Table 1 The Free volume parameters and T_g of membranes.

Membrane	I_3 (%)	τ_3 (ns)	r_3 (nm)	FFV (%)	T_g (°C)
SPEEK	8.828	2.408	0.320	0.988	161.8
SPEEK/GO-8	9.364	2.476	0.325	1.080	176.7
SPEEK/GO-DA-8	9.240	2.271	0.309	0.954	172.3
SPEEK/GO-DA-Cys-2	8.570	2.415	0.320	0.989	165.1
SPEEK/GO-DA-Cys-4	9.620	2.431	0.322	1.003	172.9
SPEEK/GO-DA-Cys-6	9.560	2.341	0.314	1.081	174.9
SPEEK/GO-DA-Cys-8	9.770	2.292	0.310	1.116	180.3

The errors were all less than 4%.

3.3 Gas separation performance

3.3.1 Effect of water uptake

The gas permeability of glassy SPEEK polymer is very low in dry state. All the membranes are fully humidified before gas permeation tests. Time-dependent mixed gas CO_2 separation properties of unfilled SPEEK and SPEEK/GO-DA-Cys-8 membranes are shown in Fig. S2 (see supporting materials). The water uptake has a tremendous influence on the gas permeability of SPEEK membrane (Fig. 6 and Fig. S3). The increased swelling of membranes increases the intermolecular distance between the polymer chains, and thus is beneficial to gas transport as reported previously.[45,59,60] All gas permeabilities (CO_2, CH_4 and N_2) increase when the water content is lower than 18 wt % due to the increased intermolecular distance between the polymer chains. The CH_4 and N_2 permeabilities decrease when the total water content is higher than 18 wt % due to the following reason. The introduction of cysteine and dopamine in humidified membranes brings abundant CO_2 sorption sites that only react with CO_2 but not with CH_4 and N_2. The high bound water content as shown in Table S4 leads to a relatively lower transport resistance to CO_2 than to CH_4 and N_2. The relationship between CO_2/gas selectivity and bound water content proves the fact that bound water facilitates the hydration of CO_2 which can permeate through the membrane with a much lower energy barrier, thus leading to a high CO_2/gas selectivity.

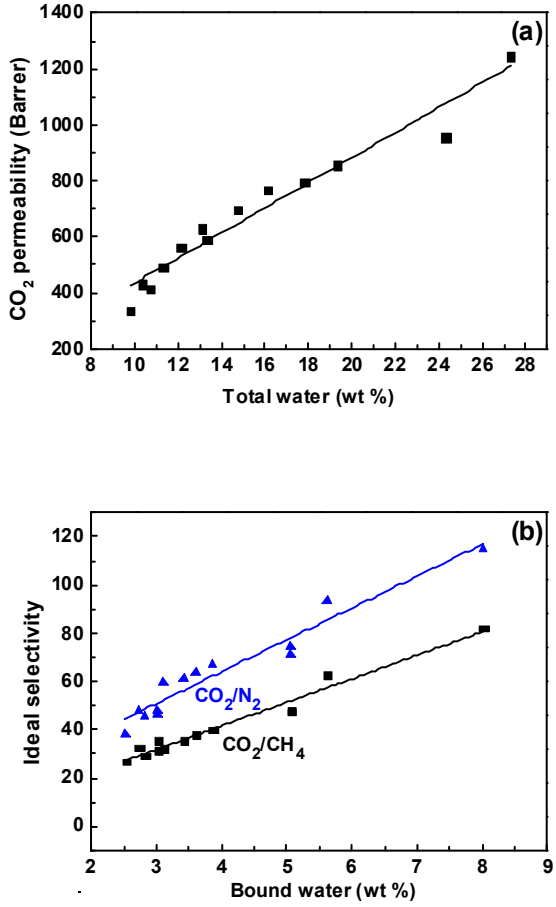

Fig. 6. (a) Correlations between pure gas CO_2 permeability and total water and (b) Correlations between pure gas CO_2/CH_4, CO_2/N_2 selectivity and bound water in membranes (1 bar, 25 ^oC).

3.3.2 Pure gas separation performance

The solubility coefficient (S) and diffusivity coefficient (D) of pure gas are measured in dry state for comparison (Table 2). The CO_2/CH_4 and CO_2/N_2 diffusivity selectivities of composite membranes increase with increasing GO-DA-Cys loading in comparison with unfilled SPEEK membrane. The GO sheet structure with a high aspect ratio leads to the highly tortuous diffusion paths for the larger molecule in polymer matrix, and the increased tortuosity is beneficial to increase diffusivity selectivity. The order of gas diffusivity is related to the size of molecular kinetic diameters, and the kinetic diameter of gas is in the order CO_2 (3.3 Å) < N_2 (3.6 Å) < CH_4 (3.8 Å).[61,62] Thus, CO_2/CH_4 diffusivity selectivity is higher than CO_2/N_2 diffusivity selectivity due to the larger molecular size difference between CO_2 and CH_4.

The solubility-controlled membrane separates gases according to their relative condensability which is characterized by critical temperature.[61] The critical temperature of gases follows the sequence of CO_2 (304.2 K) > CH_4 (190.7 K) > N_2 (126.1 K).[61,62] The higher condensability results in the higher solubility of gas in polymer. CO_2/CH_4 and CO_2/N_2 solubility selectivities of composite membranes doped with amino acid-functionalized GO are higher than that of composite membranes doped with dopamine modified GO. The increased solubility selectivity is attributed to the introduction of cysteine, which contains a carboxylic acid group and an amine group with an excellent affinity for polar CO_2. In addition, CO_2/N_2 solubility selectivity is higher than CO_2/CH_4 solubility selectivity due to the larger condensability difference between CO_2 and N_2.

In humidified state, the selectivity of SPEEK/GO-DA membrane is significantly higher than that of SPEEK/GO membrane. It is attributed to the enhancement of reactivity selectivity resulted from the specific, reversible reaction between CO_2 molecules and amine carriers. It can be seen that SPEEK/GO-DA-Cys-8 membrane presents a CO_2 permeability of 1247 Barrer with selectivities of 81.8 and 114.5 for CO_2/CH_4 and CO_2/N_2, respectively (Table 3).

For SPEEK/GO-DA-Cys composite membranes in humidified state, both permeability and selectivity are significantly enhanced after humidification and increase with increasing nanosheet contents (Table 3). The increase in CO_2 permeability can be attributed to the following reasons. The improved gas permeability is the comprehensive effect of the increased water uptake, the increased amine groups, the increased FFV, the decreased crystallinity and the decreased gas diffusivity coefficient. First, water uptake plays an important role in SPEEK/GO-DA-Cys composite membranes. With the increase of water uptake, both the solubility and the diffusivity of CO_2 increase, and therefore the CO_2 permeability increases. Second, the reaction between CO_2 and amine carriers is greatly promoted under humidified conditions, and thus the CO_2 permeability increases with the increasing amount of amine carriers in the membrane. Third, since the FFV of the SPEEK/GO-DA-Cys composite membranes increases and crystallinity of composite membranes decreases compared with SPEEK/GO and SPEEK/GO-DA composite membranes, the CO_2 permeability increases. In addition, the decreased gas diffusivity coefficient mainly due to the increased tortuosity diffusion paths for gas molecular leads to reduced CO_2 permeability.

Compared with SPEEK/GO and SPEEK/GO-DA composite membranes, the SPEEK/GO-DA-Cys composite membranes show the highest CO_2/CH_4 (N_2) selectivity due to the following reasons. Firstly, the presence of amine groups on GO sheet surface is able to enhance the amino acid functionalized graphene oxide's affinity toward CO_2. As the amount of amine groups increases, the conversion of CO_2 into HCO_3^- is more favored attributed to the enhancement of reactivity selectivity resulted from the specific, reversible reaction between CO_2 molecules and amine carriers.

Secondly, the solubility selectivity is increased with the increasing of GO-DA-Cys content. The increased solubility selectivity is due to the introduction of carboxylic acid groups and amine groups, which have excellent affinity for polar CO_2. Moreover, CO_2/N_2 solubility selectivity is higher than CO_2/CH_4 solubility selectivity due to the larger condensability difference between CO_2 and N_2. Thirdly, compared with unfilled SPEEK membrane, the more tortuous diffusion paths for the larger molecule as well as the increased chain rigidification in composite membranes lead to increased CO_2/gas diffusivity selectivity. In summary, for SPEEK/GO-DA-Cys composite membranes, the combination of diffusivity selectivity, solubility selectivity and reactivity selectivity successfully improves the CO_2/gas selectivity.

Table 2 Pure gas diffusion and solubility coefficients of dry membranes (membranes were tested at 1.5 bar, 25 °C).

Membrane	D_{CO2}[a]	D_{CH4}[a]	D_{N2}[a]	S_{CO2}[b]	S_{CH4}[b]	S_{N2}[b]	D_{CO2}/D_{CH4}	D_{CO2}/D_{N2}	S_{CO2}/S_{CH4}	S_{CO2}/S_{N2}
SPEEK	5.00	1.42	1.94	3.11	0.41	0.21	3.53	2.57	7.56	14.76
SPEEK/GO-2	4.56	1.21	1.62	3.22	0.42	0.23	3.77	2.81	7.62	13.91
SPEEK/GO-4	4.18	1.08	1.46	3.31	0.42	0.22	3.88	2.86	7.86	15.01
SPEEK/GO-6	3.62	0.88	1.08	3.42	0.43	0.26	4.11	3.32	7.91	13.08
SPEEK/GO-8	4.48	1.03	1.42	3.10	0.43	0.24	4.37	3.16	7.21	12.92
SPEEK/GO-DA -2	5.09	1.42	1.98	3.31	0.42	0.21	3.59	2.58	7.86	15.71
SPEEK/GO-DA-4	5.03	1.43	1.70	3.59	0.42	0.24	3.54	2.96	8.57	15.01
SPEEK/GO-DA-6	4.90	1.37	1.55	4.00	0.43	0.26	3.58	3.15	9.30	15.38
SPEEK/GO-DA-8	4.67	1.20	1.38	4.31	0.44	0.27	3.87	3.38	9.77	15.93
SPEEK/GO-DA-Cys-2	4.97	1.39	1.91	3.60	0.44	0.22	3.57	2.60	8.18	16.36
SPEEK/GO-DA-Cys-4	4.74	1.15	1.86	4.18	0.48	0.22	4.13	2.54	8.54	18.64
SPEEK/GO-DA-Cys-6	4.20	1.01	1.57	4.91	0.48	0.25	4.14	2.68	10.21	19.60
SPEEK/GO-DA-Cys-8	4.05	0.93	1.38	5.51	0.49	0.27	4.35	2.94	11.22	20.37

[a]Diffusivity coefficient [cm^2/s] × 10^8 [b]Solubility coefficient [cm^3(STP)/cm^3cmHg]× 10^2
The errors were all less than 10%.

Table 3 Comparison of pure gas transport properties of the dry membranes and humidified membranes.

Membrane	Dry membrane			Humidified membrane		
	P_{CO2}(Barrer)	$\alpha_{CO2/CH4}$	$\alpha_{CO2/N2}$	P_{CO2} (Barrer)	$\alpha_{CO2/CH4}$	$\alpha_{CO2/N2}$
SPEEK	15.5	26.7	38.0	565.3	26.6	38.1
SPEEK/GO-2	14.6	28.7	39.2	493.2	29.2	39.3
SPEEK/GO-4	13.8	30.5	42.9	335.2	31.1	42.8
SPEEK/GO-6	12.3	32.5	43.5	292.6	32.7	43.6
SPEEK/GO-8	13.9	31.5	40.8	432.7	32.2	41.8
SPEEK/GO-DA -2	16.8	28.2	40.5	590.5	31.2	46.1
SPEEK/GO-DA-4	18.1	30.3	44.4	698.4	35.4	61.5
SPEEK/GO-DA-6	19.6	33.3	48.5	798.3	39.7	67.2
SPEEK/GO-DA-8	20.1	37.8	53.8	856.2	47.8	74.5
SPEEK/GO-DA-Cys-2	17.9	29.2	42.5	631.1	35.2	48.1
SPEEK/GO-DA-Cys-4	19.4	35.3	47.4	771.9	47.4	71.5
SPEEK/GO-DA-Cys-6	20.6	42.3	52.5	957.8	62.7	93.2
SPEEK/GO-DA-Cys-8	22.3	48.8	59.8	1247.6	81.8	114.5

The errors were all less than 10%.

3.3.3 Mixed gas separation performance

Binary gas mixtures of CO_2/CH_4 (CO_2/CH_4 = 30/70 vol%) and CO_2/N_2 (CO_2/N_2 = 10/90 vol%) are used to evaluate the performance of composite membranes under industrial relevant conditions. The mixed gas permeability and separation factor results for the composite membranes are shown in Fig. 7. The separation factors obtained under mixed gas conditions are slightly lower than the ideal selectivity values. This difference in selectivity between mixed and pure gas measurements is a well-known phenomenon and is mainly ascribed to the effects of penetrant competitive sorption. However, the mixed gas CO_2 permeability, CO_2/CH_4 and CO_2/N_2 separation factors of composite membranes doped with GO-DA-Cys are similar to the corresponding ideal gas permeation properties. It is the fact that the introduction of cysteine and dopamine in membranes bring the abundant CO_2 sorption sites, which can only react with CO_2. Therefore, the presence of a second gas (CH_4 or N_2) has little effect on the permeability of CO_2.

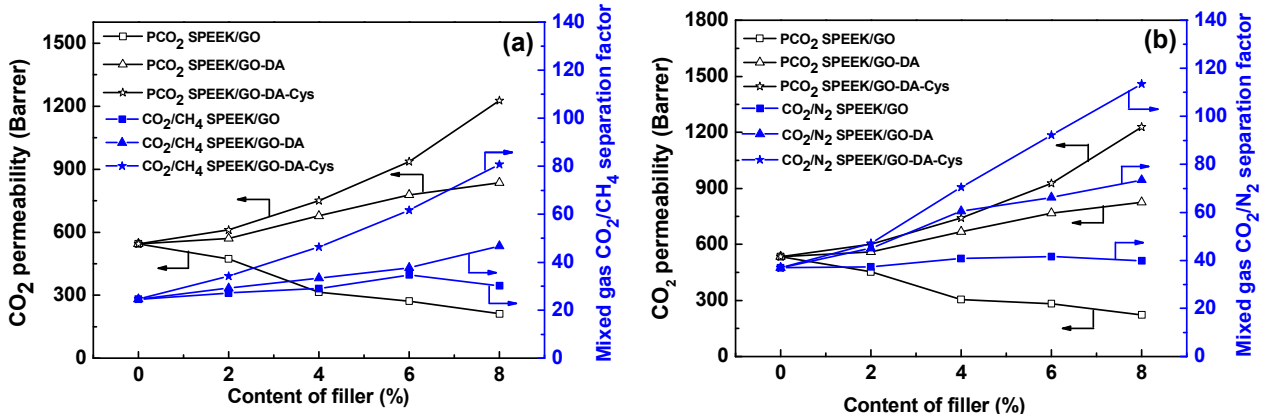

Fig. 7. (a) Mixed gas CO_2 (CO_2/CH_4 = 30/70 vol%) permeability and CO_2/CH_4 separation factor; (b) Mixed gas CO_2 (CO_2/N_2 = 10/90 vol%) permeability and CO_2/N_2 separation factor for GO, GO-DA and GO-DA-Cys nanosheets based composite membranes (1 bar, 25 °C).

3.3.4 Effect of operating temperature

The effect of operating temperature on membrane separation performance is investigated for MMMs containing non-functional and functional GO nanosheets as well as unfilled SPEEK membrane as shown in Fig. 8. Generally, for a glassy polymer, the diffusivity increases with temperature due to the increased flexibility of the polymer chains. Consequently, the permeabilities of gases (CO_2, CH_4 and N_2) gradually increase with temperature, while the separation factors of CO_2/CH_4 and CO_2/N_2 decrease.

The temperature dependence of gas permeability can be further described by using the Arrhenius equation which relates the gas permeability to the operating temperature *via* the activation energy (E_p) of permeability as expressed by the following equation (6):

$$P = P_0 \exp\left(-\frac{E_p}{RT}\right) \quad (6)$$

where P, P_0, R and T are the permeability of the gas, the pre-exponential factor, the gas constant and the absolute temperature, respectively. The activation energies (E_P) of permeability calculated from the slope of ln$P$ vs 1000/T are 24.69, 19.54, 10.68 and 9.30 kJ/mol for unfilled SPEEK, SPEEK/GO-8, SPEEK/GO-DA-8 and SPEEK/GO-DA-Cys membranes, respectively. E_P has a significantly drop in MMMs incorporated with GO-DA-Cys at the loading of 8 % compared with unfilled SPEEK.

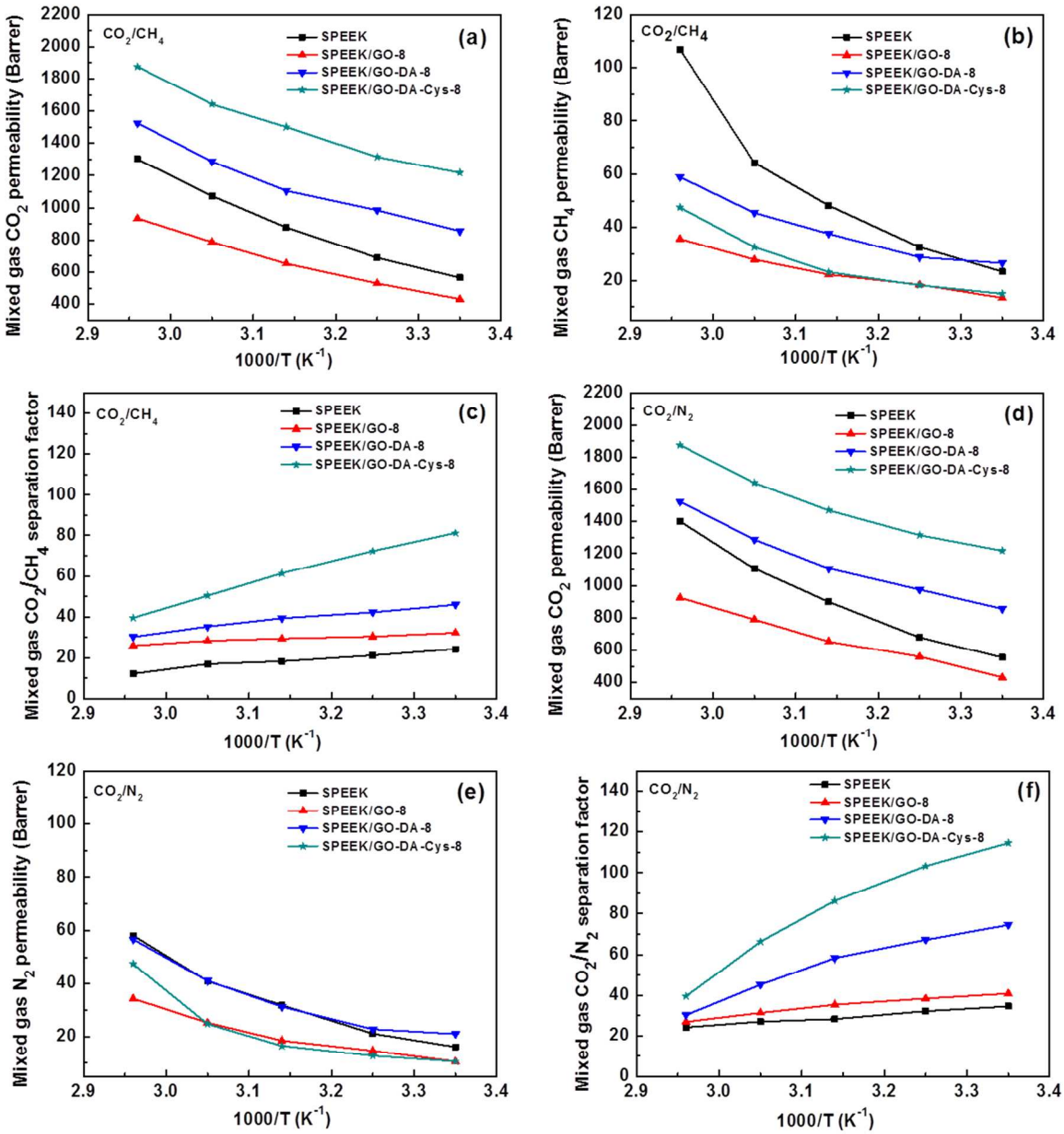

Fig. 8. Effect of operating temperature on (a) Mixed gas CO_2 (CO_2/CH_4 = 30/70 vol %) permeability; (b) Mixed gas CH_4 permeability; (c) Mixed gas CO_2/CH_4 separation factor; (d) Mixed gas CO_2 (CO_2/N_2 = 10/90 vol %) permeability; (e) Mixed gas N_2 permeability; (f) Mixed gas CO_2/N_2 separation factor of membranes in mixed feed gases. Permeation tests were performed at 1 bar feed pressure with humidified feed gas and sweep gas.

3.3.5 Comparison of gas separation performance in this study with reported in literatures

The gas separation performance of some typical CO_2-facilitated transport fillers incorporated composite membranes reported in literatures and composite membranes gas separation results achieved in this study are summarized for CO_2/CH_4 and CO_2/N_2 mixture, respectively (Fig. 9 and Table S5). It can be noticed that the separation performance of composite membranes is comparable with composite membranes reported in literatures in humidified state, surpassing the Robeson upper bound revised in 2008.

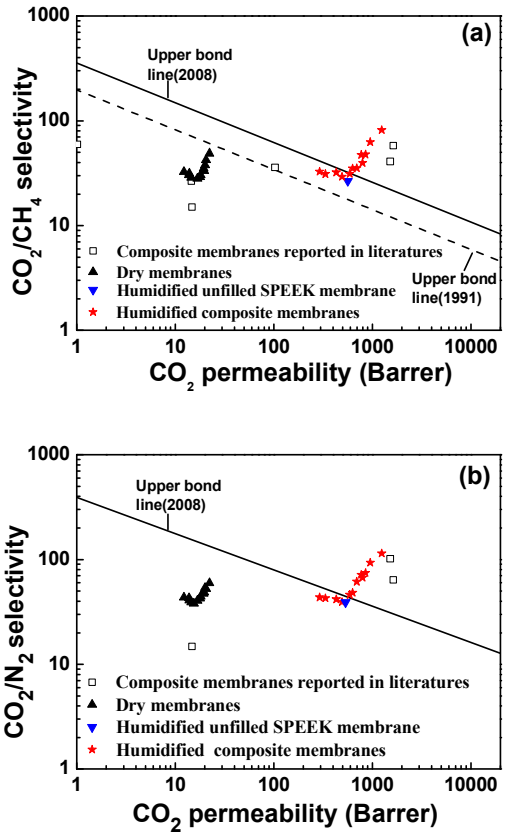

Fig. 9. Pure gas separation performance of the membranes for (a) CO_2/CH_4 and (b) CO_2/N_2 mixtures, respectively (temperature: 25 °C; pressure: 1 bar).

3.3.6. Long-term operation stability

The long-term operation stability of membrane is vital for industrial application. The operation stability of the SPEEK/GO-DA-Cys-8 composite membrane is investigated up to 120 h for CO_2/N_2 mixture at 1 bar feed pressure and 65 °C (Fig. 10). The CO_2 permeability and the CO_2/N_2 separation factor remain stable during the entire test period.

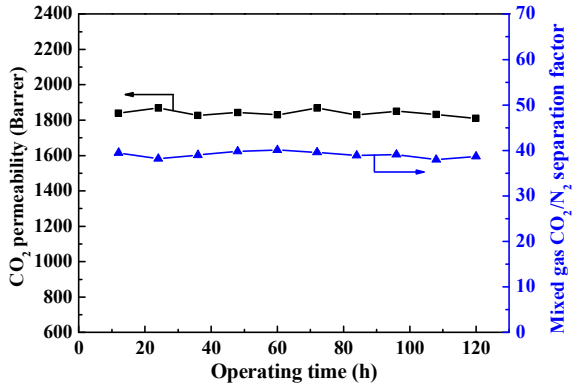

Fig. 10. The long-term gas separation performance test of the SPEEK/GO-DA-Cys-8 composite membrane up to120 h for CO_2/N_2 mixture at 1 bar feed pressure and 65 °C with humidified feed gas and sweep gas.

4. Conclusion

Composite membranes are fabricated by incorporating amino acid-functionalized GO nanosheets for gas separation. The introduction of GO nanosheets leads to more tortuous paths for the larger molecules, enhancing diffusivity selectivity. Furthermore, the amino acid with carboxyl groups and amino groups simultaneously enhances solubility selectivity and reactivity selectivity of CO_2/CH_4 and CO_2/N_2. These composite membranes are endowed with enhanced CO_2 separation performance. Compared with unfilled SPEEK membrane, the highest CO_2/CH_4 and CO_2/N_2 selectivities of 82 and 115 for SPEEK/GO-DA-Cys-8 membrane are increased by 171% and 131%, respectively, with a CO_2 permeability of 1247 Barrer at 1.0 bar and 25 °C. These results surpass 2008 Robeson upper bound and the as-prepared composite membranes are promising for CO_2 separation.

Appendix for the abbreviation list

T_g	Glass transition temperatures (°C)
r_3	Free volume radius (nm)
τ_3	Lifetime of *o*-Ps (ns)
I_3	Intensity of *o*-Ps component (%)
FFV	Apparent fractional free volume (%)
Δr	Electron layer thickness (nm)
W_d	Weight of dry membranes (mg)
W_w	Weight of a fully hydrated membrane at constant temperature (mg)
m_1	The weight of membrane after gas permeation test (mg)
m_2	The weight of membrane after 100 °C in a vacuum oven to remove free water (mg)
m_0	The weight of membrane after 150 °C in a vacuum oven to remove bound water (mg)
W_t	Content of total water (%)
W_f	Content of free water (%)
W_b	Content of bound water (%)
W_{dry}	The weight of dry membrane (mg)
W_{wet}	The weight of fully hydrated membrane (mg)
A_{dry}	The area of dry membrane (cm^2)
A_{wet}	The area of fully hydrated membrane (cm^2)
P_i	Permeability of each gas (Barrer)
Q_i	Volumetric flow rate of gas 'i' (cm^3/s (SPT))
l	Thickness of the membranes (μm)
Δp_i	Transmembrane pressure difference gas constant (cmHg)
$\alpha_{i/j}$	Ideal selectivity and mixed gas separation factor of gas 'i and j'
D	Diffusion coefficient ($[cm^2/s] \times 10^8$)
S	Solubility coefficient ($[cm^3(STP)/cm^3cmHg] \times 10^2$)
E_p	The activation energy of permeability (kJ/mol)
SPEEK	Sulfonated poly(ether ether ketone)
GO	Graphene oxide
DA	Dopamine
Cys	Cysteine

Acknowledgements

The authors gratefully acknowledge the financial support from the National High Technology Research and Development Program of China (2012AA03A611), Program for New Century Excellent Talents in University (NCET-10-0623), the National Science Fund for Distinguished Young Scholars (No.21125627) and the Program of Introducing Talents of Discipline to Universities (B06006).

Notes and references

[a]*Key Laboratory for Green Chemical Technology, School of Chemical Engineering and Technology, Tianjin University, Tianjin 300072, China*
[b]*Collaborative Innovation Center of Chemical Science and Engineering (Tianjin), Tianjin 300072, China*

[c]Tianjin Key Laboratory of Membrane Science and Desalination Technology, Tianjin University, Tianjin 300072, China
[d]Tianjin Institute of Pharmaceutical Research, Tianjin 300193, China
[e]Key Laboratory of Nuclear Radiation and Nuclear Energy Technology, Institute of High Energy Physics, Chinese Academy of Sciences, Beijing 100049, China

1. M. D. Guiver and Y. M. Lee, *Science,* **2013**, *339,* 284–285.

2. D. L. Gin and R. D. Noble, *Science,* **2011**, *332,* 674–676.

3. L. M. Robeson, *J. Membr. Sci.,* **1991**, *62*, 165–185.

4. B. D. Freeman, *Macromolecules*, **1999**, *32*, 375–380.

5. T. S. Chung, L. Y. Jiang and S. Kulprathipanja, *Prog. Polym. Sci.,* **2007**, *32*, 483–507.

6. D. Q. Vu, W. J. Koros and S. J. Miller, *J. Membr. Sci.,* **2003**, *211*, 311–334.

7. Y. Li, G. He, S. Wang, S. Yu, F. Pan, H. Wu and Z. Jiang, *J. Mater. Chem. A,* **2013**, *35*, 10058–10077.

8. L. M. Robeson, *J. Membr. Sci.,* **2008**, *320,* 390–400.

9. Y. Zhang, J. Sunarso, S. M. Liu and R. Wang, *Int. J. Greenhouse Gas Control*, **2013**, *12*, 84–107.

10. Y. F. Li, Q. P. Xin, H. Wu, R. L. Guo, Z. Z. Tian,; Y. Liu,; S. F. Wang, G.
W. He, F. S. Pan and Z. Y. Jiang, *Energy Environ. Sci.,* **2014**, *7,* 1489–1499.

11. S. Zhao, Z. Wang, Z. H. Qiao, X. Wei, C. X. Zhang, J. X. Wang and Wang, S. C. *J. Mater. Chem. A,* **2013**, *1,* 246–249.

12. W. Yave, A. Car and K. V. Peinemann, *J. Membr. Sci.,* **2010**, *350,* 124–129.

13. O. G. Nik, X. Y. Chen and S. Kaliaguine, *J. Membr. Sci.,* **2011**, *379,* 468–478.

14. T. W. Pechar, M. Tsapatsis, E. Marand and R. Davis, *Desalination,* **2002**, *146,* 3–9.

15. A. Car, C. Stropnik and K. V. Peinemann, *Desalination,* **2006**, *200,* 424–426.

16. J. Ahmad and M. B. Hägg, *J. Membr. Sci.,* **2013**, *445,* 200–210.

17. L. Y. Jiang, T. S. Chung, C. Cao, Z. Huang and S. Kulprathipanja, *J. Membr. Sci.,* **2005**, *252,* 89–100.

18. T. W. Pechar, S. Kim, B. Vaughan, E. Marand, M. Tsapatsis, H. K. Jeong and C. J. Cornelius, *J. Membr. Sci.,* **2006**, *277,* 195–202.

19. A. Galve, D. Sieffert, C. Staudt, M. Ferrando, C. Guell, C. Téllez, and J. Coronas, *J. Membr. Sci.,* **2013**, *431,* 163–170.

20. M. Anson, J. Marchese, E. Garis, N. Ochoa and C. Pagliero, *J. Membr. Sci.,* **2004**, *243,* 19–28.

21. A. F. Ismail, P. S. Goh, S. M. Sanip and M. Aziz, *Sep. Purif. Technol.,* **2009**, *70*, 12–26.

22. Y. Zhang, I. H. Musselman, J. P. Ferraris and K. J. Balkus, *J. Membr. Sci.,* **2008**, *313,* 170–181.

23. H. W. Kim, H. W. Yoon, S. M. Yoon, B. M. Yoo, B. K. Ahn, Y. H. Cho, H. J. Shin, H. Yang, U. Paik, S. Kwon, J. Y. Choi and H. B. Park, *Science,* **2013**, *342,* 91–95.

24. H. Li, Z. Song, X. Zhang, Y. Huang, S. Li, Y. Mao, H. J. Ploehn, Y. Bao and M. Yu, *Science,* **2013**, *342,* 95–98.

25. S. Choi, J. Coronas, E. Jordan, W. Oh, S. Nair, F. Onorato, D. F. Shantz and M. Tsapatsis, *Angew., Chem. Int. Ed.,* **2008**, *47,* 552–555.

26. J. Choi and M. Tsapatsis, *J. Am. Chem. Soc.,* **2010**, *132,* 448–449.

27. C. Rubio, C. Casado, P. Gorgojo, F. Etayo, S. Uriel, C. Téllez and J. Coronas, *Eur. J. Inorg. Chem*., **2010**, 159–163.

28. A. Galve, D. Sieffert, E. Vispe, C. Téllez, J. Coronas and C. Staudt, *J. Membr. Sci.,* **2011**, *370,* 131–140.

29. M. X. Shan, Q. Z. Xue, N. N. Jing, C. C. Ling, T. Zhang, Z. F. Yan and J. T. Zheng, *Nanoscale*, **2012**, *4,* 5477–5482.

30. P. S. Goh, A. F. Ismail, S. M. Sanip, B. C. Ng and M. Aziz, *Sep. Purif. Technol.,* **2011**, *81,* 243–264.

31. J. Shen, G. P. Liu, K. Huang, W. Q. Jin, K. R. Lee and N. P. Xu, *Angew. Chem., Int. Ed*., **2014**, *53*, 1–6.

32. C. F. Yang, W. H. Smyrl and E. L. Cussler, *J. Membr. Sci.*, **2004**, *231*, 1–12.

33. Z. P. Smith and B. D. Freeman, *Angew. Chem., Int. Ed.,* **2014**, *53,* 10286–10288.

34. R. K. Joshi, P. Carbone, F. C. Wang, V. G. Kravets, Y. Su, I. V. Grigorieva, H. A. Wu, A. K. Geim and R. R. Nair, *Science,* **2014**, *343,* 752–754.

35. S. Kasahara, E. Kamio and H. Matsuyama, *J. Membr. Sci.,* **2014**, *454,* 155–162.

36. S. Kasahara, E. Kamio, T. Ishigami and H. Matsuyama, *J. Membr. Sci.,* **2012**, *415–416,* 168–175.

37. S. Kasahara, E. Kamio, A. Yoshizumi and H. Matsuyama, *Chem. Commun.,* **2014**, *50*, 2996–2999.

38. D. F. Guo, H. Thee, C. Y. Tan, J. Chen, W. Y. Fei, S. Kentish, G. W. Stevens and G. Silva., *Energy Fuels,* **2013**, *27*, 3898−3904.

39. X. F. Wang, N. G. Akhmedov, Y. H. Duan, D. Luebke and B. Y. Li, *J. Mater. Chem. A,* **2013**, *1*, 2978–2982.

40. R. Dawson, D. J. Adams and A. I. Cooper, *Chem. Sci.,* **2011**, *2*, 1173–1177.

41. M. Wang, Z. Wang, S. Li, C. Zhang, J. Wang and S. Wang, *Energy Environ. Sci.,* **2012***, 6*, 539–551.

42. X. Duan, R. J. Song, J. C. Yu, H. L. Wang, Y. J. Cui, Y. Yang, B. L. Chen and G. D. Qian, *RSC Advances,* **2014**, *4*, 36419–36424.

43. D. H. Hong and M. P. Suh, *Chem. Eur. J.,* **2014**, *20*, 426–434.

44. Y. Zhang, Z. Wang and S. C. Wang, *J. Appl. Polym. Sci.,* **2002**, *86*, 2222–2226.

45. L. A. El-Azzami and E. A. Grulke, *J. Membr. Sci.,* **2009**, *328*, 15–22.

46. S. Li, Z. Wang, X. Yu, J. Wang and S. Wang, *Adv. Mater.,* **2012**, *24,* 3196–3200.

47. H. Matsuyama, A. Terada, T. Nakagawara, Y. Kitamura and M. Teramoto, *J. Membr. Sci.,* **1999**, *163,* 221–227.

48. Y. N. Zhao and W. S. W. Ho, *J. Membr. Sci.,* **2012**, *415-416,* 132–138.

49. J. Huang, J. Zou and W. S. W. Ho, *Ind. Eng. Chem. Res.,* **2008**, *47,* 1261–1267.

50. J. Zou and W. S. W. Ho, *J. Membr. Sci.,* **2006**, *286,* 310–321.

51. Q. P. Xin, J. Y. Ouyang, T. Y. Liu, Z. Li, Z. Li, Y. C. Liu, S. F. Wang, H. Wu, Z. Y. Jiang and X. Z. Cao, *ACS Appl. Mater. Interfaces,* **2014**, DOI: 10.1021/am504742q.

52. Y. Liu, D. D. Peng, G. W. He, S. F Wang, Y. F. Li, H. Wu and Z. Y. Jiang, *ACS Appl. Mater. Interfaces,* **2014**, *15,* 13051–13060.

53. Q. P. Xin, H. Wu, Z. Y. Jiang, Y. F. Li, S. F. Wang, Q. X. Li, Q. Li, X. Lu, X. Z. Cao and J. Yang, *J. Membr. Sci.,* **2014**, *467,* 23–35.

54. A. L. Khan, C. Klaysom, A. Gahlaut, X. F. Li and I. F. J. Vankelecom, *J. Mater. Chem.,* **2012**, *22,* 20057–20064.

55 W. S. Hummers Jr and R. E. Offeman, *J. Am. Chem. Soc.* **1958**, *80,* 1339–1339.

56 H. S. Lee, M. Dellatore, W. M. Miller and P. B. Messersmith, *Science,* **2007**, *318,* 426–430.

57. B. G. Choi, J. Hong, Y. C. Park, D. H. Jung, W. H. Hong, P. T. Hammond and H. Park, *ACS Nano,* **2011***, 5,* 5167–5174.

58. Y. Lian, Y. Liu, T. Jiang, J. Shu, H. Lian and M. Cao, *J. Phys. Chem. C,* **2010***, 114,* 9659–9663.

59. Y. F. Li, S. F. Wang, G. W. He, H. Wu, F. S. Pan and Z. Y. Jiang, *Chem. Soc. Rev.,* **2015**, *44*, 103–118.

60. S. Shishatskiy, J. R. Pauls, S. P. Nunes and K. V. Peinemann, *J. Membr. Sci.,* **2010**, *359,* 44–53.

61. D. R. Lide, CRC Handbook of Chemistry and Physics: A Ready Reference Book of Chemical and Physical Data, CRC Press, Cleveland, 2004.

62. S. Matteucci, Y. Yampolskii, B. D. Freeman and I. Pinnau, Transport of Gases and Vapors in Glassy and Rubbery Polymers, John Wiley & sons, New York, 2006.

The table of contents entry

Amino acid-functionalized graphene oxide nanosheets-incorporated composite membranes significantly enhanced $CO_2/CH_4(N_2)$ diffusivity, reactivity and solubility selectivity.